Applied Catalysis B: Environmental 305 (2022) 121037

Contents lists available at ScienceDirect

Applied Catalysis B: Environmental

journal homepage: www.elsevier.com/locate/apcatb

An isotopic strategy to investigate the role of water vapor in the oxidation of 1,2-dichloroethane over the Ru/WO_3 or Ru/TiO_2 catalyst

Xiaohui Yu [a], Lingyun Dai [b], Jiguang Deng [a,*], Yuxi Liu [a], Lin Jing [a], Xing Zhang [a], Ruyi Gao [a], Zhiquan Hou [a], Lu Wei [a], Hongxing Dai [a,*]

[a] Beijing Key Laboratory for Green Catalysis and Separation, Key Laboratory of Beijing on Regional Air Pollution Control, Key Laboratory of Advanced Functional Materials, Education Ministry of China, Laboratory of Catalysis Chemistry and Nanoscience, Department of Environmental Chemical Engineering, School of Environmental and Chemical Engineering, Faculty of Environment and Life, Beijing University of Technology, Beijing 100124, China
[b] John A. Paulson School of Engineering and Applied Sciences, Harvard University, Cambridge, Massachusetts 02138, United State

ARTICLE INFO

Keywords:
Supported ruthenium catalyst
1,2-dichloroethane oxidation
Isotopic trace
Water vapor effect
Reaction intermediate

ABSTRACT

Electron paramagnetic resonance, in situ diffuse reflection infrared Fourier transform spectroscopy, and temperature-programmed techniques by means of the isotopic trace strategies were used to investigate the effects of water vapor on oxygen species, reaction pathways, byproducts distributions, and accumulation of the chlorine and carbon species on the catalyst surface for 1,2-dichloroethane oxidation over Ru/WO_3 or Ru/TiO_2 catalyst. The introduction of water vapor produced the OOH species that were converted into more active oxygen (O_2^- and O^-) species. The mulliken population analysis indicates that βC and αC in VC are bonded with H and nucleophilic oxygen of −OH in sequence, respectively, which proved that water directly promoted the transformation of vinyl chloride to CH_3COOH. Besides, water could be partially adsorbed at the hydroxyl groups on the Ru/WO_3 sample surface, which were provided the adsorption sites for 1,2-dichloroethane molecules. However, the severe competitive adsorption on the surface of Ru/TiO_2 resulted in insufficient oxygen adsorption to supplement the oxygen vacancy.

1. Introduction

Chlorinated volatile organic compounds (CVOCs) are a kind of gaseous pollutants with strong toxicity, high chemical stability, and difficult degradation nature harmful to the atmosphere environment and human health [1,2]. 1,2-Dichloroethane (1,2-DCE) is one of the typical CVOCs, which are emitted from vinyl chloride (VC) production [3], pharmaceuticals manufacturing industry [4], coating and printing processes [4], metal degreasing [5], and petrochemical industry. At present, catalytic oxidation is one of the effective pathways to remove low-concentration CVOCs [6,7]. There has been a lot of catalysts focused on the combustion of CVOCs. For example, transition-metal oxides (MO_x; M = Mn [8], Ce [9], Cr [10], V [11], and W [12]) are relatively cheap and good thermal stability, but long-term exposure to the chlorine species produced by CVOCs combustion processes can easily lead to occupation of the active sites and hence deactivation of the catalysts employed. Therefore, the researchers have proposed a series of strategies to improve the catalytic performance of MO_x, such as loading precious metals [13,14], doping other transition-metal oxides [15,16], and modifying with acid or base materials [17], among which the Ru-based catalysts were efficient for the destruction of chlorinated organics because of excellent redox performance and strong anti-toxic ability [17–22]. On the one hand, Ru, as a cheaper precious metal than platinum and palladium, is a promising alternative which can reduce the cost of industrial applications; on the other hand, supported Ru catalysts show a high dechlorination efficiency in the oxidation of CVOCs, while Pt and Pd often combine with the Cl species, resulting in the loss of the active sites and rapid deactivation of the catalysts. In particular, the Cl species produced by the C−Cl bond cleavage during the CVOCs oxidation process could effectively be removed from the supported Ru catalyst surface as Cl_2 through the Deacon reaction (i.e., the Cl species was oxidized to Cl_2: $4HCl + O_2 \rightarrow 2H_2O + 2Cl_2$). At 250 °C or higher temperatures, the supported catalysts, such as Ru/Al_2O_3 [23], Ru/Co_3O_4 [14], and Ru/CeO_2 [8], exhibited high and stable performance for the Deacon reaction involved in the oxidation of 1,2-dichloroethane, dichlorobenzene or chlorobenzene. For example, the Ru/TiO_2 and Ru/WO_3 catalysts possessed a good resistance to chlorine poisoning, in which Ru/TiO_2 has been applied as an industrial catalyst for the

* Corresponding authors.
E-mail addresses: jgdeng@bjut.edu.cn (J. Deng), hxdai@bjut.edu.cn (H. Dai).

https://doi.org/10.1016/j.apcatb.2021.121037
Received 10 October 2021; Received in revised form 13 November 2021; Accepted 20 December 2021
Available online 23 December 2021
0926-3373/© 2021 Elsevier B.V. All rights reserved.

Deacon reaction. The acidity of WO_3 and TiO_2 are very important in the catalytic elimination of CVOCs.

Water plays an important role in the oxidation of VOCs, which is usually attributed to the following three points: (i) Effective removal of the chlorine and carbon species because of the cleaning effect [24,25]. The H^+ produced by water combines with Cl^- on the surface of the catalyst to form HCl, since the catalysts are prone to adsorb more amounts of OH than of chlorine species [26]; (ii) the increase in amount of the basic OH due to adsorb more amounts of O atoms from water [27], which can facilitate the interaction of OH with Cl atoms in 1,2-DCE molecules [28], and OH favors the adsorption and transfer of oxygen on the MO_x catalysts, which is important during HCHO oxidation [29]; and (iii) the reverse reaction of the Deacon process is easy to occur in the presence of water, which improves the selectivity to HCl [30]. More generally speaking, however, the introduction of water often leads to the decrease of reactivity, which is believed to be caused by the competitive adsorption of water and oxygen or reactant molecules at the active centers [12,26]. Some researchers have also proposed that the introduction of water reduces the amount of medium and strong acids, especially the amount of the Brønsted acid sites [31].

In one of our previous works [32], we found that the promoting effect of water on the reaction was mainly attributed to the production of $^{16}O^{18}O$, which directly participated in the reaction. Therefore, H_2O plays a more important role in catalytic oxidation as a precursor to new reactive oxygen species, and oxygen in water participates in the exchange with the adsorbed oxygen and lattice oxygen. However, effects of the new active oxygen species on the products distribution and reaction pathways of CVOCs oxidation have not been clear up to now. Based on the excellent performance of the Ru-based catalysts for the oxidation of CVOCs in the presence of water, the present work is focused on the following two aspects: (i) How does the oxygen provided by water participate in the oxidation of 1,2-DCE? and (ii) what is the decisive factor to promote or inhibit 1,2-DCE oxidation in the presence of water? and does the introduction of water influence the reaction mechanism? Therefore, electron paramagnetic resonance (EPR), isotope trace, and in situ diffuse reflection infrared Fourier transform spectroscopic (in situ DRIFTS) techniques were used to investigate the role of water in products distribution and reaction pathways of 1,2-DCE oxidation over the Ru/WO_3 and Ru/TiO_2 catalysts.

2. Experimental

2.1. Catalyst preparation

The Ru/WO_3 and Ru/TiO_2 samples were prepared by the $NaBH_4$ reduction method. The typical preparation process was as follows: A certain amount of $RuCl_3$ aqueous solution (0.01 mol/L) was added to the poly vinyl alcohol (PVA; 2.0 g/L, Ru/PVA mass ratio = 1.0: 1.2) solution, and then 0.5 g of WO_3 or TiO_2 was impregnated under stirring for 6 h. After that, a certain amount of $NaBH_4$ aqueous solution (2.0 g/L) was quickly added to the above mixed solution under stirring for 20 min (Ru/PVA molar ratio = 1.0: 5.0), followed by adding 15 mL of ammonium hydroxide under vigorously stirring for another 20 min (just for Ru/WO_3) to transform $[RuCl_6]^{2-}$ ions into the $[(NH_3)_4Ru]^{2+}$ ions, which were effectively deposited on the surface of WO_3. Then, the mixed solution was filtered under vacuum, dried in an oven at 80 °C for 24 h, and calcined in an air flow of 100 mL/min at 500 °C for 2 h, thus obtaining the Ru/WO_3 and Ru/TiO_2 samples, respectively. The theoretical loadings of Ru in Ru/WO_3 and Ru/TiO_2 were 2.0 wt%, and the actual loadings determined by the inductively coupled plasma—atomic emission spectroscopic (ICP—AES) technique were 1.4 and 1.5 wt%, respectively.

2.2. Catalyst characterization

The ICP—AES, electron paramagnetic resonance (EPR), temperature-programmed experiments (TPSR, TPD and TPO), in situ diffuse reflection infrared Fourier transform spectroscopy (in situ DRIFTS), X-ray photoelectron spectroscopy (XPS), and Fourier transfer infrared (Py-FTIR) spectroscopy were used to characterize physicochemical properties of the samples. The detailed characterization procedures can be seen in the Supplementary data. The computational methodology and model for density functional theory (DFT) calculations were described in the Supplementary material.

2.3. Catalytic performance evaluation

Catalytic performance evaluation of the samples for 1,2-DCE oxidation was carried out in a continuous flow fixed-bed quartz micro-reactor. A thermoelectric couple was used to measure the reaction temperatures in the middle of the micro-reactor, in which 0.55 g of quartz sands (40–60 mesh) was well mixed with 50 mg of the catalyst (40–60 mesh) to avoid the hot spots possibly produced by the formation heat of 1,2-DCE oxidation. The reactant gas stream of 33.3 mL/min in actual conditions was composed of (1000 ppmv 1,2-DCE + 20 vol% O_2 + N_2 (balance)), giving a space velocity (SV) of ca. 40,000 mL/(g h). A water saturator kept at 33.5 °C was used to introduce 5.0 vol% water vapor to the reaction system. The heating belt (the temperature was kept at 105 °C) was used to reduce the possible adsorption of the 1,2-DCE or by-products on the inner pipe surface. The concentrations of reactants and products were online measured using a GC-7890B (Agilent) apparatus, and the 1,2-DCE conversion was calculated according to the formula of $(c_{in} - c_{out})/c_{in} \times 100\%$ (the c_{in} and c_{out} are the inlet and outlet 1,2-DCE concentrations, respectively). Every activity datum was an average value determined at a given temperature for three times, and the standard deviations were within 0.4%. Cl_2 was determined using the chemical titration with ferrous ammonium sulfate as reducing agent and *N*,*N*-diethyl-*p*-phenylenediamine as an indicator. The Cl balance throughout the reaction system was estimated to 98.0 ± 2.0%.

3. Results and discussion

3.1. Effect of water vapor on catalytic performance

Fig. 1 A shows catalytic activities of the WO_3 and Ru/WO_3 samples for 1,2-DCE oxidation in the presence or absence of 5.0 vol% water vapor. It is apparent that the addition of water vapor led to decreases in reaction temperatures $T_{50\%}$ and $T_{90\%}$ (corresponding to 1,2-DCE conversions of 50% and 90%) over the Ru/WO_3 sample of 15 °C (from 300 to 285 °C) and 20 °C (from 340 to 320 °C), respectively, and a drop in $T_{50\%}$ over the WO_3 sample of 15 °C (from 345 to 330 °C). The results indicate that water vapor introduction improved the activity of WO_3 and Ru/WO_3 for 1,2-DCE oxidation. The distributions of C_2H_3Cl (VC, the main product of 1,2-DCE oxidation) detected by GC are shown in Fig. 1B. The contents of VC were detected for 1,2-DCE oxidation over Ru/WO_3 in the presence of water to be less than 20 ppm in the whole temperature range, but the introduction of water vapor made the VC decomposition temperature from higher than 400 °C in the absence of water vapor to 320 °C over the WO_3 sample, manifesting that water vapor promoted the transformation of the intermediate product.

3.2. Effect of water vapor on formation of the oxygen species

Due to the variable valence states of W in WO_3, there are oxygen vacancies with different concentrations, which are dependent on the conditions of the sample preparation. In view of the different effects of water vapor on 1,2-DCE oxidation over the catalysts, we first evaluated the changes of oxygen species before and after water vapor was introduced to the catalyst system, which would be very important in understanding the involved reaction mechanisms. Fig. 2 presents EPR spectra of the samples. A significant enhanced signal was found at $g = 2.003$ on the Ru/WO_3 sample (Fig. 2A), which was due to the oxygen

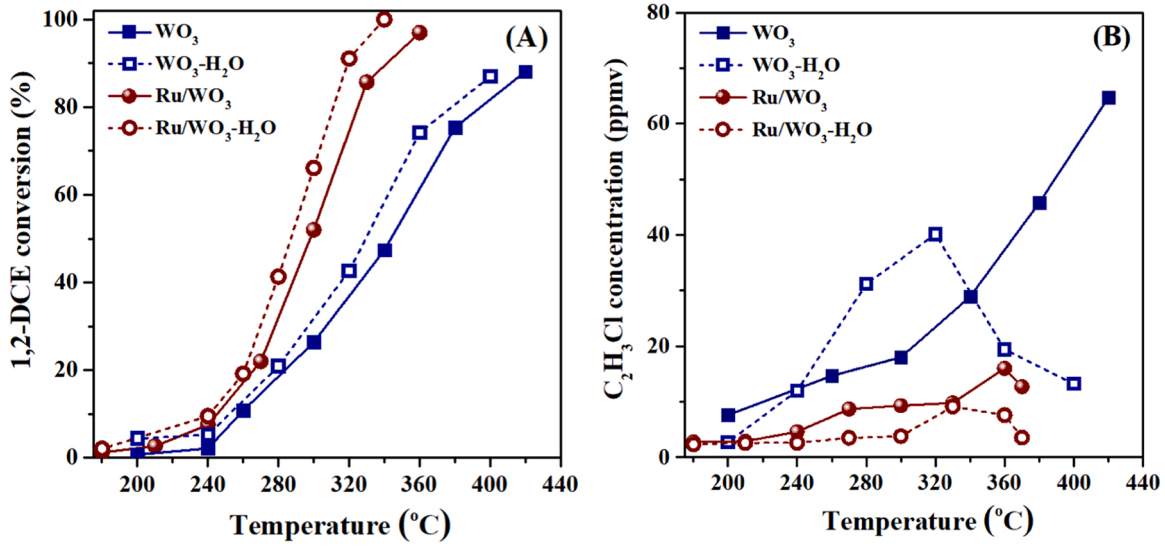

Fig. 1. (A) Catalytic activities and (B) C_2H_3Cl concentration of the WO_3 and Ru/WO_3 samples for 1,2-DCE oxidation in the presence or absence of water vapor at SV = 40,000 mL/(g h).

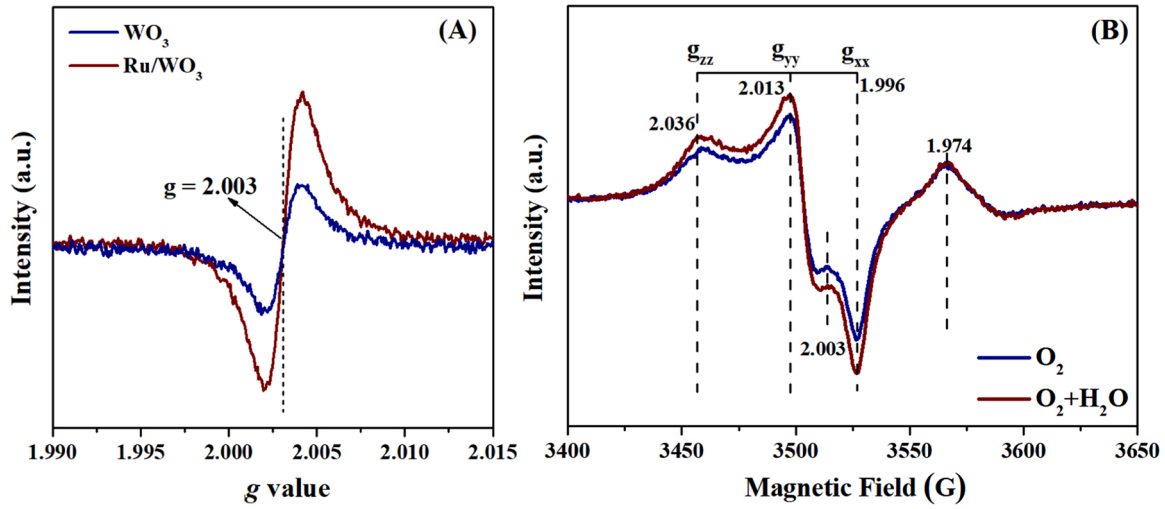

Fig. 2. EPR spectra of (A) WO_3 and Ru/WO_3 and (B) Ru/WO_3 in O_2 and (O_2 + H_2O) streams, respectively.

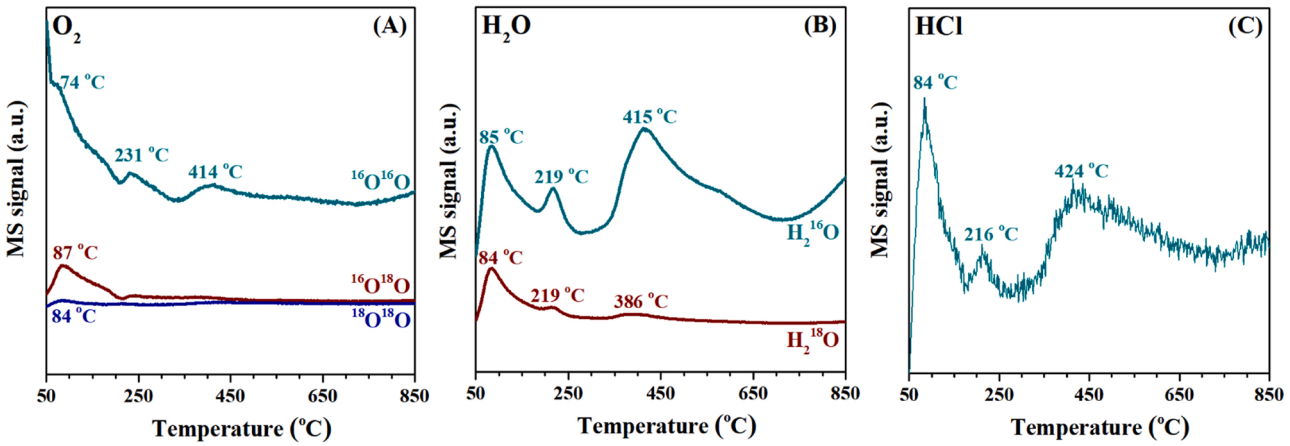

Fig. 3. . (A) O_2, (B) H_2O, and (C) HCl desorption in the 1,2-DCE-TPD profiles of (A) O_2, (B) H_2O, and (C) HCl over the WO_3 sample in the presence of $H_2{}^{18}O$.

vacancy corresponding to the electron capture of oxygen defect. This result indicates that Ru/WO_3 possessed a higher concentration of oxygen vacancies. Fig. 2B shows the EPR spectra of the Ru/WO_3 catalyst with light illumination obtained at − 196 °C in O_2 or (O_2 + H_2O) stream. The strong signals were assigned to the paramagnetic superoxide anion (O_2^-) formed on the Ru/WO_3 surface, which were stabilized at the $W^{\delta+}$ sites (g_{xx} = 1.996, g_{yy} = 2.013, and g_{zz} = 2.036) [33,34]. The signals emerging at g = 2.003 were associated with the characteristic Ru^{3+} species, accompanied by the production of more hole-trapped O^- species [35]. Specifically, the EPR signals of O_2^- were strengthened once water vapor was introduced, signifying that there were more amounts of the O_2^- and O^- species at even − 196 °C.

The isotope trace technique was used to figure out why more amounts of the O_2^- and O^- species were produced. The 1,2-DCE-TPD experiments in the presence or absence of $H_2{}^{18}O$ were carried out, and the desorbed species were detected by a mass spectrometer. The formation of $^{16}O^{18}O$ species was observed in our previous work on Ru/3DOM WO_x. Not surprisingly, desorption of $^{16}O^{18}O$ was also observed in this work on WO_3 (Fig. 3A). According to the formation temperature of HCl, we can exclude the influence of the carbon impurity species accumulated on the surface of the sample to judge the degree of reaction. HCl desorption (84, 216, and 424 °C) occurred at similar temperatures for the desorption of the $^{16}O^{16}O$ (74, 231, and 414 °C) and $H_2{}^{16}O$ (85, 219, and 415 °C) species. O_2 desorption at 400 °C could be considered to be due to the lattice oxygen, and that below 400 °C was assigned to the desorption of the adsorbed oxygen species on the WO_3

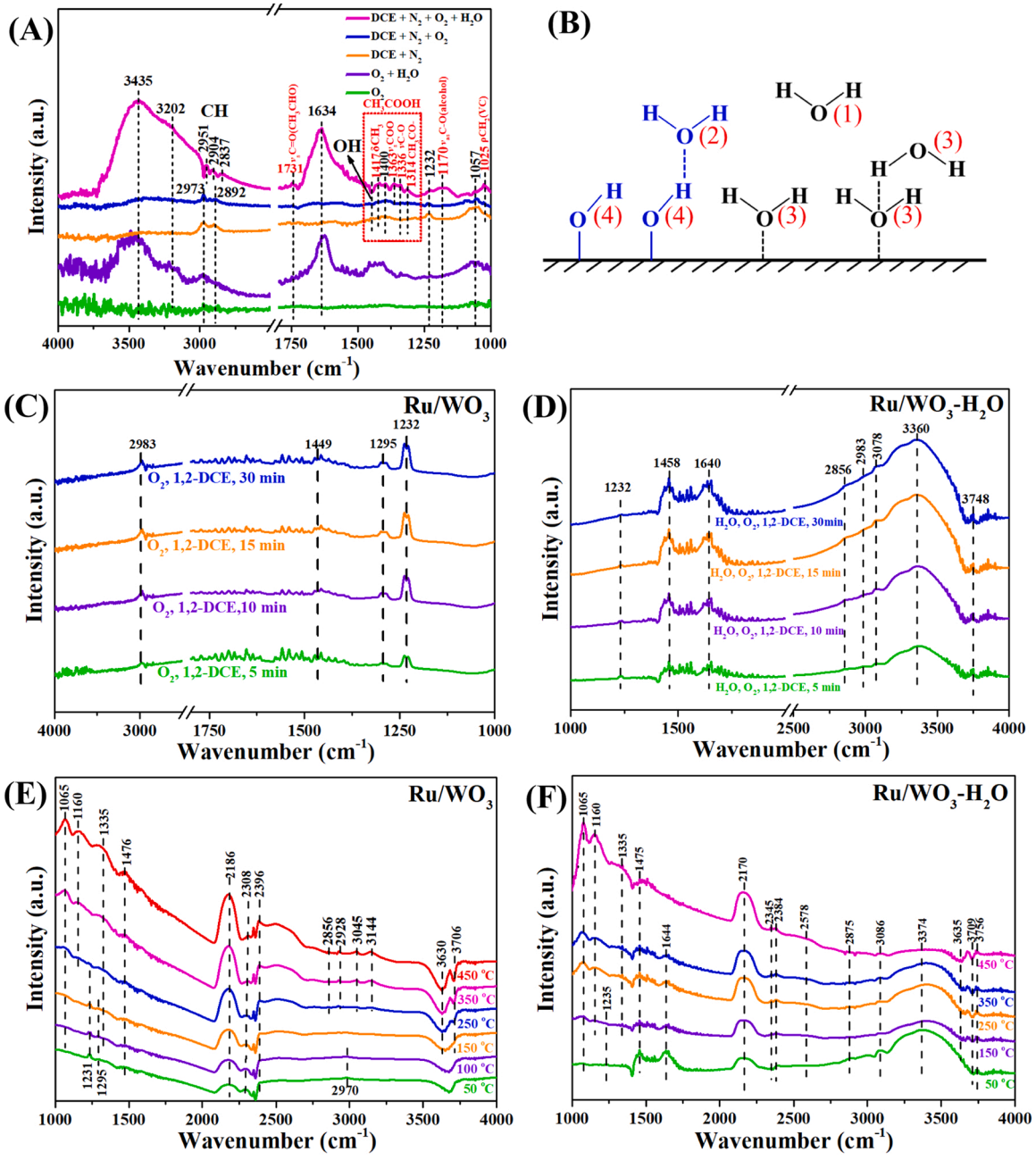

Fig. 4. In situ DRIFTS spectra of (A) the Ru/WO_3 sample in different atmospheres at room temperature, (B) schematic illustration of four types of hydroxyl groups on the sample surface, in situ DRIFTS spectra of the Ru/WO_3 sample (C) in a flow of (1,2-DCE + O_2) for 30 min, (D) in a flow of (1,2-DCE + O_2 + H_2O) for 30 min, and (E, F) in a flow of (1,2-DCE + O_2) in the absence and presence of water vapor at different temperatures, respectively. Reaction conditions: 1000 ppmv 1,2-DCE, 20 vol % O_2, 5.0 vol% H_2O, N_2 (balance), and a total flow rate of 30 mL/min.

surface. It is obvious that both the adsorbed oxygen and lattice oxygen species played important roles in 1,2-DCE oxidation. By tracking the ^{18}O in the oxygen-containing by-products, we can find desorption of $CH_3C^{16}O^{18}OH$ and a small amount of $CH_3C^{18}O^{18}OH$ at 210 °C, which resulted in the generation of $C^{16}O^{18}O$ and almost no generation of $C^{18}O^{18}O$ (Fig. S1). The decomposition of the carbonate species above 500 °C to produce $CH_3C^{16}O^{18}OH$ suggests that such an oxygen exchange took place in the lattice oxygen. This result demonstrates that the introduction of water vapor exchanged not only with the adsorbed oxygen on the surface of the WO_3 sample, but also with the lattice oxygen, although no desorption peaks at temperatures higher than 500 °C of $C^{18}O^{18}O$ or $C^{16}O^{18}O$ were recorded. We believe that the exchange of one oxygen atom resulted in formation of $^{16}O^{18}O$, rather than $^{18}O^{18}O$, although Dai et al. [28] found that the exchange in water could be either one or two oxygen atoms. In addition, no signals of dichloroethane, vinyl chloride, and dichloromethane were recorded in the mass spectrum after water vapor was added, which might be caused by the competitive adsorption of water and these species.

Combined with the results of 1,2-DCE-TPD and EPR characterization after introduction of the isotope $H_2{}^{18}O$, we think that the promotional effect of water addition on 1,2-DCE oxidation over Ru/WO_3 was mainly due to the oxygen exchange between the adsorbed H_2O and the O_2 adsorbed on the sample surface or lattice oxygen, resulting in the O_2^- and O^- species that could promote the oxidation of 1,2-DCE. According to the trend of VC formation over WO_3, the introduction of water vapor provided a more amount of the active adsorbed oxygen ($^{16}O^{18}O$) species, which promoted the oxidation of 1,2-DCE to VC. Furthermore, $H_2{}^{18}O$ isotope experiments prove that a more amount of the oxygen isotopes was consumed to produce the intermediate species of $CH_3C^{16}O^{18}OH$ (Fig. S1(D)).

3.3. Effect of water vapor on the reaction pathway

Fig. 4 shows the in situ DRIFTS spectra of the Ru/WO_3 sample under the different conditions. The influence of oxygen on the adsorption of 1,2-DCE and water molecules was studied. As shown in Fig. 4A, when the sample was exposed to O_2, the signal due to the superoxide (O_2^-) species (at 1074 cm^{-1}) was not detected [36], indicating that the sample had a weak adsorption of oxygen at room temperature. After the introduction of water vapor, the characteristic bands at 3435 and 3202 cm^{-1} were attributed to the hydrogen-bond water, the ones at 1634 and 1458 cm^{-1} were the O−H bending and stretching vibration modes of the adsorbed water, and the one at 1057 cm^{-1} was assigned to the methoxy group [37]. Compared with the spectra of the sample in the (1,2-DCE + N_2) or (1,2-DCE + N_2 + O_2) flow, the introduction of O_2 slightly weakened the adsorption of 1,2-DCE (at 1232, 2973, and 2892 cm^{-1}). In the presence of water vapor, the obvious C═O symmetric stretching band of aldehydes at 1731 cm^{-1}, anti-symmetric C−O stretching band of alcohols at 1170 cm^{-1}, $\rho(CH_2)$ of VC at 1025 cm^{-1}, and the band of the carbonate species at 1300 − 1450 cm^{-1} were observed. Fig. 4C–F shows the in situ DRIFTS spectra of the Ru/WO_3 sample after adsorption and reaction in the absence or presence of water vapor. Under the anhydrite condition, the negative bands at 3630 and 3706 cm^{-1} were attributed to the bridging acidic OH and isolated basic OH, and became stronger in intensity with a rise in temperature. The depletion of the acidic hydroxyl group was due to the fact that the 1,2-DCE molecules adsorbed at oxygen vacancies were attacked by the OH adjacent to the W atom to form the carbocation. That is to say, the adsorption of 1,2-DCE in hydroxyl group was enhanced. The depletion of the basic hydroxyl group was owing to the fact that 1,2-DCE molecules adsorbed on the Lewis acid sites were attacked by the basic OH to form $-O-CH_2CH_2Cl$. After introduction of water vapor, the adsorption of 1,2-DCE was not changed, but some new vibration bands of free OH groups at 3748 cm^{-1}, hydrogen-bonded OH at 3360 cm^{-1}, hydrogen group at 1630 and 1458 cm^{-1}, and characteristic band attributable to the $\nu_s(CH_2)$ at 3078 cm^{-1} were recorded [37,38]. With the rise in temperature, the characteristic band of hydrogen-bond water at 3374 cm^{-1} weakly adsorbed on the sample surface was decreased gradually in intensity [29], but the free OH groups at 3756 cm^{-1} were relatively stable and could not be desorbed from the surface of the sample even at high temperatures. Fig. 4B schematically illustrates these four hydroxyl groups on the Ru/WO_3 surface after water vapor addition: (i) Free OH groups (at 3756 cm^{-1}), (ii) terminal isolated basic OH (at 3709 cm^{-1}), (iii) hydrogen-bonded OH (at 3374 cm^{-1}), and (iv) bridging acidic OH (at 3635 cm^{-1}). Hence, it shows the same trend in the presence of water vapor as that under the anhydrous condition, i.e., the introduction of water vapor did not change the reaction pathways. In order to study the influence of water vapor on 1,2-DCE oxidation over the different catalysts, we prepared the Ru catalysts supported on the different commercial carriers (i.e., ZSM-5, CeO_2, TiO_2, and Al_2O_3) using the same method, and measured their activities for 1,2-DCE oxidation in the presence or absence of water vapor, as shown in Fig. S2. The results demonstrate that the introduction of water vapor exhibited a significant inhibition only over the Ru/TiO_2 catalyst. One of our previous works on Ru/3DOM WO_x and RuP/3DOM WO_x revealed that the introduction of water vapor showed an obvious promotional effect on 1,2-DCE oxidation over Ru/3DOM WO_x. As a contrast, we hence selected the Ru/TiO_2 sample to further study the inhibitive effect of water vapor on 1,2-DCE oxidation (Fig. S2), and the results reveal that water vapor exhibited a negative effect on 1,2-DCE oxidation over Ru/TiO_2. In Fig. 5A, the similar adsorption of 1,2-DCE on Ru/TiO_2 was observed, as compared with that on Ru/WO_3. The introduction of O_2 had no significant effect on the adsorption of 1,2-DCE, and obvious characteristic bands related to alcohol (at 1165 cm^{-1}), carboxylic acid (at 1250–1450 cm^{-1}), VC (at 1025 cm^{-1}), and characteristic band of the adsorbed CH_3CHO at the Lewis acid site (at 1743 cm^{-1}) [38] were observed after water vapor introduction. In the absence of water vapor, the characteristic band of hydrogen-bond OH (at 3300 cm^{-1}) was shifted to 3437 cm^{-1}. The characteristic band of CO at around 2170, 2103, and 1840 cm^{-1} were attributed to the adsorption of CO at the Lewis acid sites, and the linear adsorption and bridge adsorption states of CO on the reduced part of Ru [39,40] together with CO_2 at 2300–2400 cm^{-1} were weakened, indicating that water vapor could take away some of the carbon species on the sample surface due to its cleaning effect. From Fig. 5D and E, we can deduce that the hydrogen-bond water of the sample disassociated below 100 °C to gradually form the free water at 3727 and 3853 cm^{-1} on the surface of Ru/TiO_2 with the rise in temperature. It is worth noting that 1,2-DCE oxidation did not consume the hydroxyl groups of Ru/TiO_2, although Ru/TiO_2 possessed a more amount of hydroxyl groups than Ru/WO_3 (Fig. S3).

In conclusion, 1,2-DCE reaction pathways did not change regardless of whether water vapor promoted or inhibited the reaction, which was also proven by the results of 1,2-DCE-TPSR characterization on the Ru/WO_3 and Ru/TiO_2 samples (Figs. S4 and S5). The introduction of water vapor only further promoted the reaction pathways: 1,2-DCE → VC → alcohol → aldehyde → acetic acid. At the same time, four different hydroxyl forms on Ru/WO_3 and Ru/TiO_2 played different roles in 1,2-DCE oxidation. The hydroxyl group on the Ru/WO_3 surface and the water adsorbed on it were gradually consumed with the oxidation of 1,2-DCE, which were the active species, while only hydrogen-bond water was consumed during the reaction process over the Ru/TiO_2 sample to form free water, which was identified as inactive water.

3.4. Effect of water vapor on the products

One of our previous works reported the products distributions of 1,2-DCE oxidation in the presence or absence of water vapor over the Ru/3DOM WO_x catalysts [32]. In the present work, we studied the change of the in situ product distributions using a mass spectrometer. VC, $CHCl_3$, CCl_3CHO, and CH_3COOH were detected in the 1,2-DCE-TPSR profiles (Fig. S3) of the Ru/WO_3 sample in the presence or absence of water vapor. Interestingly, 1,2-DCE oxidation produced a large amount of

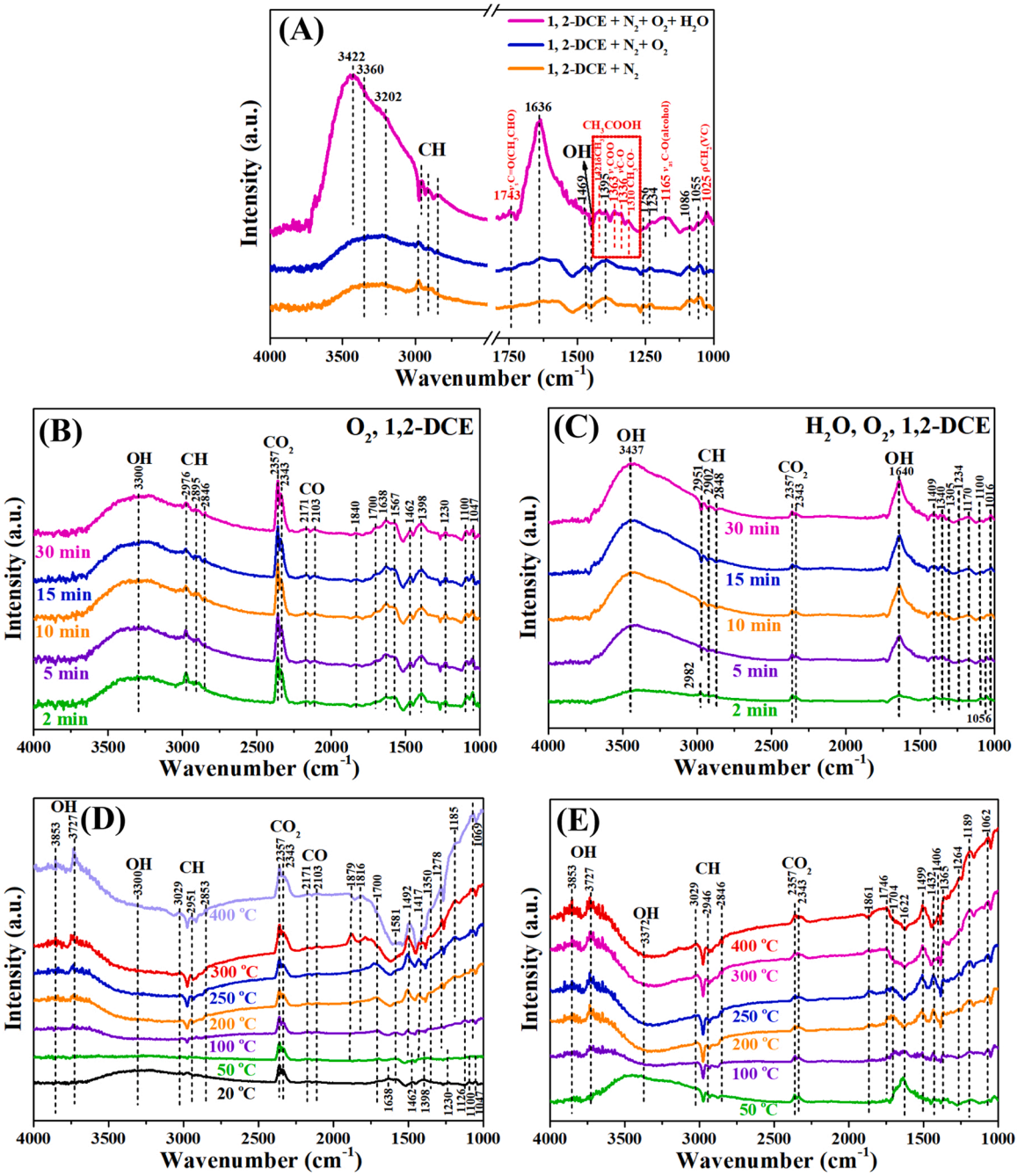

Fig. 5. In situ DRIFTS spectra of the Ru/TiO_2 sample (A) in different atmospheres at room temperature, (B) in a flow of (1,2-DCE + O_2) for 30 min, (C) in a flow of (1,2-DCE + O_2 + H_2O) for 30 min, and (D, E) in a flow of (1,2-DCE + O_2) in the absence and presence of water vapor at different temperatures, respectively. Reaction conditions: 1000 ppm 1,2-DCE, 20 vol% O_2, 5.0 vol%H_2O, N_2 (balance), and a total flow rate of 30 mL/min.

CH_3COOH in the presence of water vapor, which was completely different from that in the absence of water vapor. $H_2{}^{18}O$ and D_2O were used to track oxygen and hydrogen in the products of 1,2-DCE oxidation in the presence of water vapor using the 1,2-DCE-TPO characterization technique, and their results are shown in Fig. 6, S6, and 7, respectively. In general, ^{18}O can be traced to all of the oxygen-containing products, and D can be traced to all of the hydrogen-containing products, hence indicating that water directly participates in the reaction. It is observed that the reaction temperatures were obviously different with the substitution of H atoms in CH_3COOH and VC by different D atoms.

The hydrogen proton transfer reaction ($O_2 + H_2O \rightarrow OOH + OH$) between oxygen and water has been reported in some literature [41–45]. The OOH species shows a higher activity than the adsorbed gas-phase oxygen and can further dissociate into the reactive oxygen and hydroxyl groups. Since the O−O bond distance of OOH is 20% longer than that of gas-phase oxygen, the O−O bond in the OOH species exhibits a strong activation ability [36]. In this work, the water adsorbed at the hydroxyl group of the Ru/WO_3 sample was gradually consumed, and the isotopic ^{18}O and D were detected in each intermediate, which undoubtedly demonstrates that both the hydroxyl and OOH species generated by the reaction of water vapor and oxygen were directly involved in 1,2-DCE oxidation. Based on the theoretical calculations, Gong and coworkers concluded that 1,2-DCE oxidation first started from the rupture of the C−Cl bond, followed by the rupture of the C−H_β bond to form VC [46]. For further exploring the mechanism of water attacking VC, the Mulliken atomic charges for each atom were calculated when

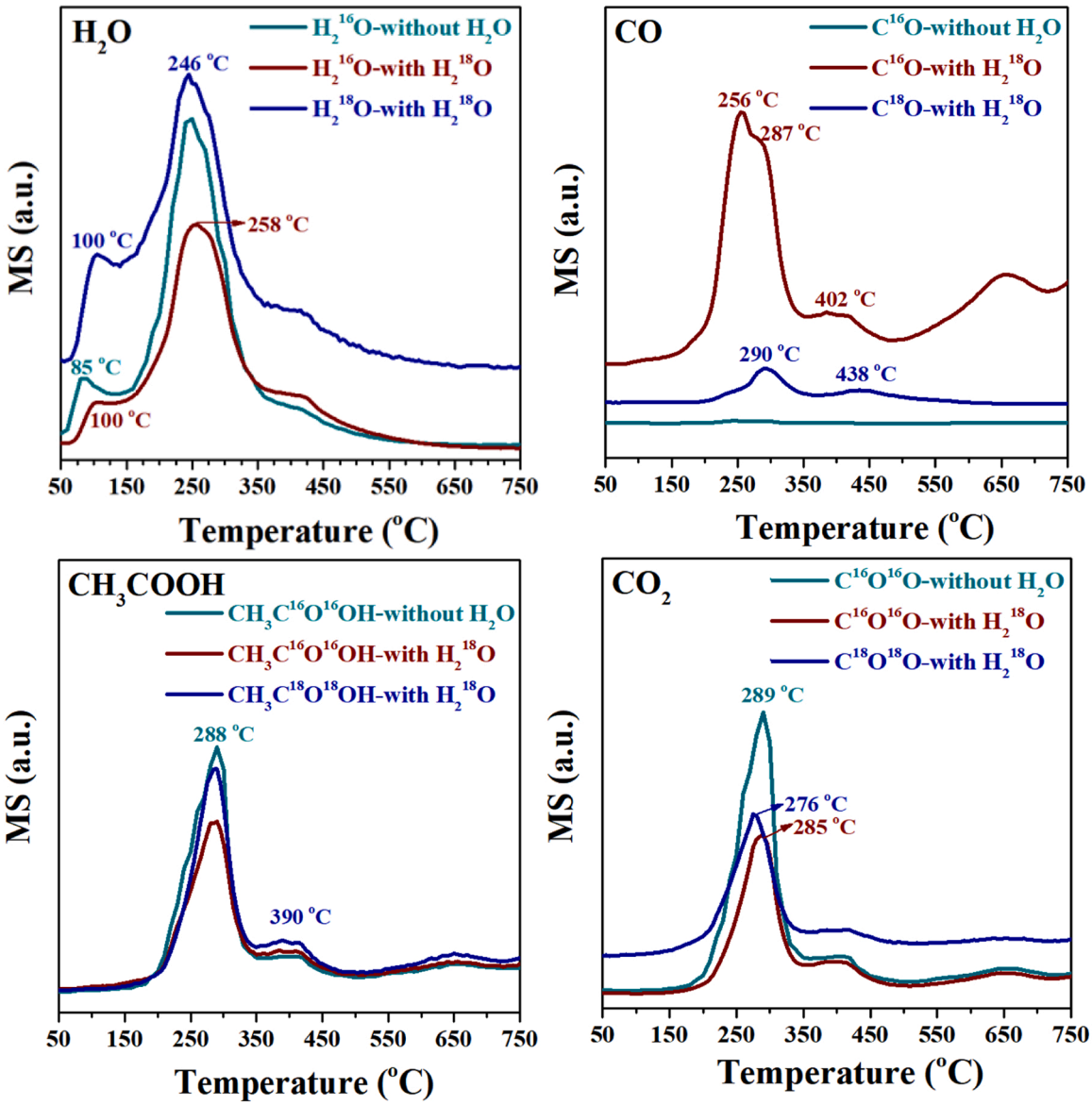

Fig. 6. H_2O, CO, CH_3COOH, and CO_2 desorption in the 1,2-DCE-TPO profiles of the Ru/WO_3 sample in the presence and absence of $H_2{}^{18}O$, respectively.

water molecule (the atoms of water marked as O7, H8, and H9) attacks different atoms of VC molecule (marked as C1, C2, H3, H4, Cl5, and H6), and the calculation results are shown in Fig. S7 and Table S1. As water approaches C2, the total charge of H_2O is − 0.037 e, higher than the negative charge when water is near the other atoms, so water has a lower potential, is more reactive, and preferentially attacks the C2 in VC molecule (when C1 is calculated, the system energy is unstable). The mulliken population analysis indicates that the charge is transferred from –OH to VC (C1 increased from −0.349 e to −0.386 e, and C2 increased from −0.079 e to –0.105 e), which are caused by the facts that C1 is bonded with H and C2 is bonded with nucleophilic oxygen in sequence. Thus, the C═C bond in VC is broken, forming an unstable carbocation with a vacant orbital, and then followed by formation of the CH_3-CHCl-O− species, which is readily oxidized to acetaldehyde and acetic acid [37]. C_2D_3Cl and C_2D_2HCl (CD_2 = CHCl or CHD = CDCl) were observed in the products (Fig. 7). It is worth noting that C_2D_3Cl appeared at 288 and 433 °C, which was different from C_2D_2HCl and C_2H_3Cl at 242 °C. The emergence of CD_2HCOOH corresponded to C_2D_3Cl attacked by the OH groups, which was due to reaction pathway II (Fig. 8), where the OH dissociated from the OOH species further reacted with the oxygen adsorbed on the surface to form the reactive oxygen species. Combined with the 1,2-DCE-TPD results, the peak at 433 °C was considered to be the lattice oxygen involved in the reaction. As shown in Fig. 6, two CO desorption peaks at 256 and 287 °C were observed, which were generated in the processes of 1,2-DCE → VC and VC → CH_3COOH, respectively. The $C^{16}O$ was formed along with the generation of VC, while the $C^{18}O$ was simultaneously formed with CH_3COOH. This was the direct evidence that oxygen in water vapor promoted the conversion of VC to CH_3COOH. At the same time, the desorption peaks of $C^{18}O$, $C^{18}O^{18}O$, and $CH_3C^{18}O^{18}OH$ at ca. 400 °C also indicates that the oxygen in water vapor exchanged with the lattice oxygen. In addition, CD_3COOH and CD_2HCOOH were also detected, but CD_3COOD was almost not detected. This result indicates that the O—D bond was more readily broken than the O—H bond in the formed acetic acid. According to the isotopic trace results of the intermediate products, 1,2-DCE oxidation pathways can be proposed, as illustrated in Fig. 9.

The following possible reactions involved in the oxygen species are shown in Fig. 8:

(a) $*O_2 + H_2{}^{18}O \rightarrow OOH + *{}^{18}OH/*O_2 + D_2O \rightarrow OOD + *OD$.

(b) $OOH \rightarrow *O + *OH/OOD \rightarrow *O + *OD$.

(c) $*OH + *O_2 \rightarrow OOH + *O/*OD + *O_2 \rightarrow OOD + *O$.

The catalyst sample possessed the O_2^- and O^- active oxygen species

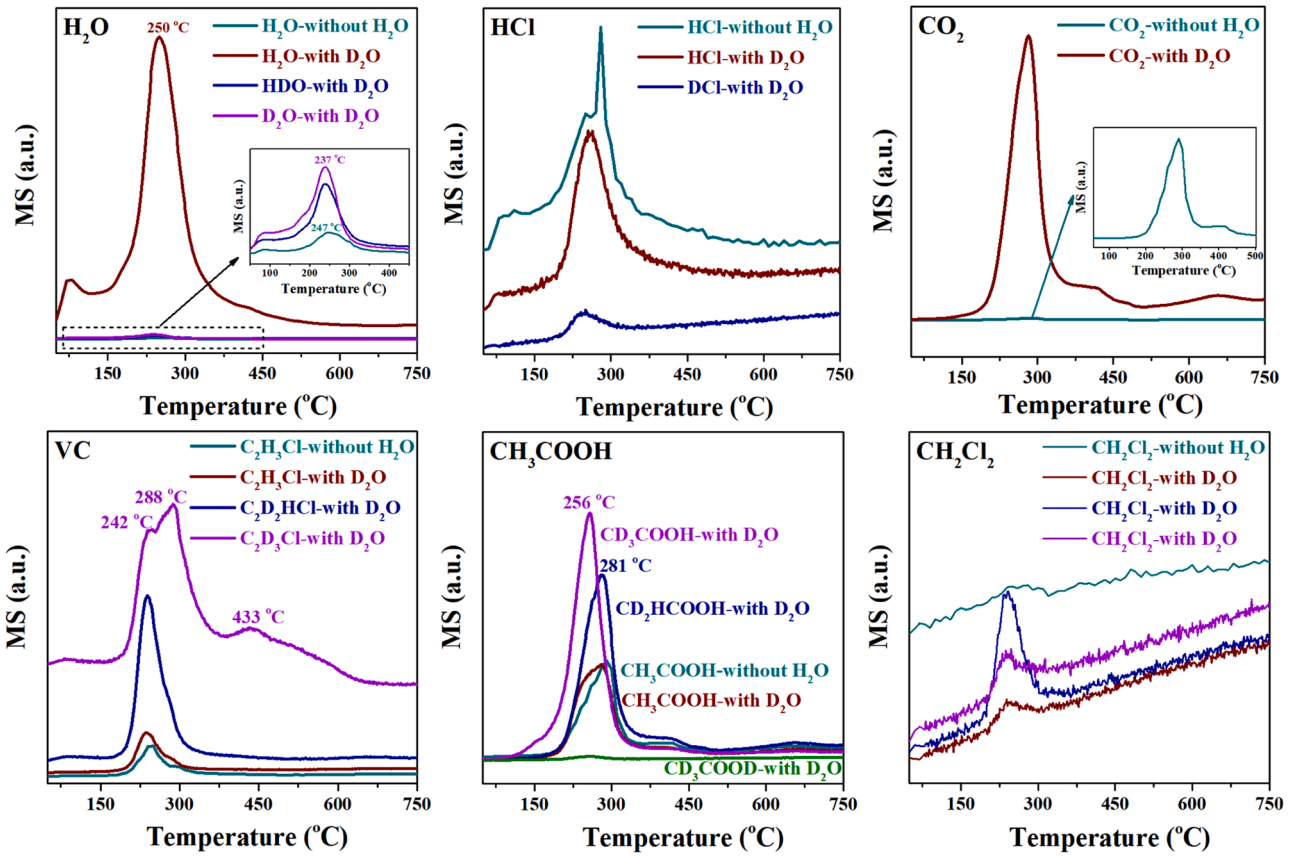

Fig. 7. H_2O, HCl, CO_2, VC, CH_3COOH, and CH_2Cl_2 desorption in the 1,2-DCE-TPO profiles of the Ru/WO_3 sample in the presence and absence of D_2O, respectively.

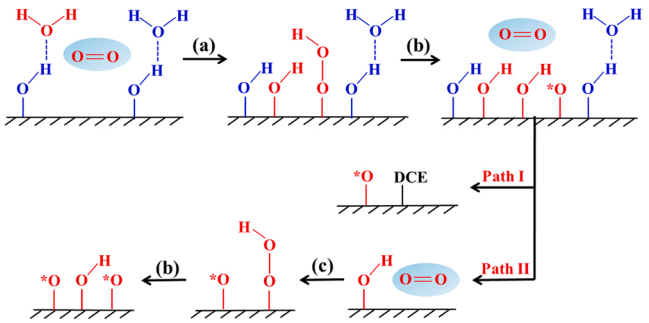

Fig. 8. Possible reaction pathways of H_2O and O_2 involvements on the surface of the Ru/WO_3 sample.

due to the electron transfer of $W^{\delta+}$ or $Ru^{\theta+}$, and the introduction of water vapor could produce new OOH/OOD species, which then decomposed into the reactive oxygen species and a hydroxyl group. Hydroxyl groups further reacted with the adsorbed oxygen to generate the reactive oxygen species, forming a more amount of the O_2^- and O^- active oxygen species (Fig. 2B). Obviously, the active oxygen species could easily exchange the oxygen with the adsorbed oxygen or lattice oxygen.

3.5. *Effects of water vapor on the accumulation of the carbon and chlorine species*

Over the Ru/WO_3 sample, the main reaction processes were as follows: (i) 1,2-DCE was first adsorbed at the oxygen vacancies and Lewis acid sites ($W^{\delta+}$ and $Ru^{\theta+}$), then the C—Cl bonds were broken and attacked by the adjacent basic terminal OH to form $-O-CH_2CH_2Cl$, and at the same time the C—C bonds were broken at the Lewis acid sites to form CH_2Cl_2; (ii) the oxygen in water was adsorbed and activated into the OOH species at the basic centers and oxygen vacancies, which was benefited from the surface hydroxyl group and isolated basic OH of the Ru/WO_3 sample; and (iii) the active oxygen (O_2^- and O^-) species attacked the reaction intermediates (VC, CH_3CHO, and etc.) adsorbed at the Lewis acid sites and oxygen vacancies, followed by the carbocation adsorbed on the bridged acidic OH was consumed, and eventually converted to CO_2, H_2O, and etc., and the oxygen vacancies were easily filled by the OH species disassembled from H_2O.

Over the Ru/TiO_2 sample, the adsorbed water mainly existed in the form of hydrogen bond due to the hydrophilicity of Ru/TiO_2, and the hydrogen-bond water was quickly removed in the heating process, accompanying by the generation of free water. The isotopic 1,2-DCE-TPD experiment (Fig. S8) reveals that the same oxygen exchange behavior led to a large amount of $CH_3C^{16}O^{18}OH$ and $C^{16}O^{18}O$. It is interesting that in the 1,2-DCE-TPD profiles, there was an obvious $^{16}O^{18}O$ desorption peak at 230 °C from the Ru/WO_3 sample, but only a weak desorption peak at 158 °C from the Ru/TiO_2 sample, indicating that the ability to convert water to the activated oxygen was weaker for Ru/TiO_2 than for Ru/WO_3. Obviously, the Mars–van Krevelen (MvK) mechanism took place over the Ru/TiO_2 sample in 1,2-DCE oxidation in view of reaction temperatures. 1,2-DCE was adsorbed at the oxygen vacancies and Lewis acid sites ($Ti^{\alpha+}$ and $Ru^{\theta+}$), and then attacked by the lattice oxygen that was rapidly replenished by the adsorbed oxygen species after depletion. In addition, the introduction of water vapor caused an obvious decrease of CH_3COOH and CO_2 concentrations in the low-temperature dechlorination. We speculate that this might be mainly due to the over-strong competitive adsorption between water vapor and oxygen, which was proven by the results of He-TPD characterization that was carried out over the samples after 10 h of stability test in the presence or absence of water vapor (Fig. S9).

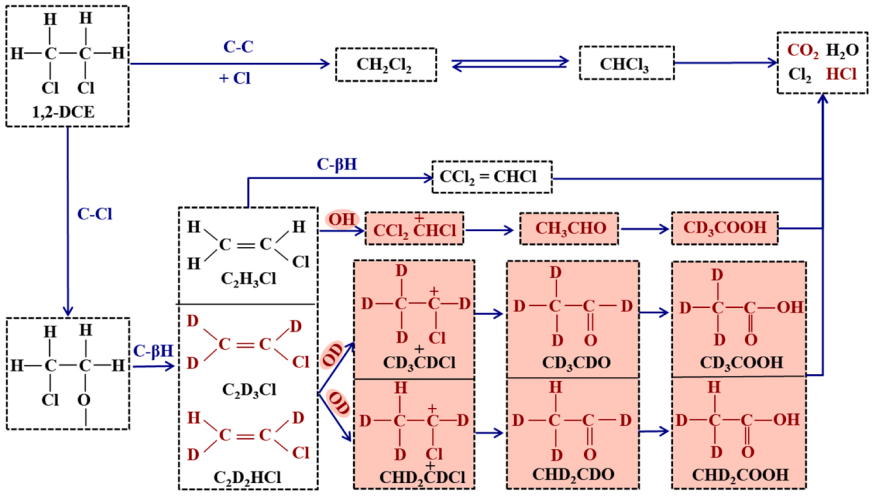

Fig. 9. Possible reaction pathways of 1,2-DCE oxidation over the samples in the presence or absence of D_2O.

The He-TPD technique was used to further study the effect of water vapor on the accumulation of the carbon and chlorine species on the Ru/WO_3 and Ru/TiO_2 surface. Firstly, there was a significant difference in desorption of O_2. After introducing water vapor, desorption of the adsorbed oxygen and lattice oxygen from Ru/WO_3 took place from 100 to 81 °C and 304 to 285 °C, respectively. However, desorption of the oxygen species at 230 °C was obviously different from that at 360 °C, reflecting that the introduction of water vapor provided the adsorbed oxygen species at 230 °C, but reduced desorption of the oxygen species at 100 °C and the lattice oxygen above 300 °C from Ru/TiO_2. Secondly, desorption peaks of Cl_2 at 286, 390, and 690 °C were observed in the presence of water vapor, which corresponded to the decomposition temperatures of VC on the Ru/WO_3 surface. Therefore, Cl_2 was believed to be formed via the oxidation of the chlorine-containing by-products accumulated on the sample surface, rather than the adsorbed chlorine gas. Although the chlorine species were oxidized above 350 °C, HCl desorption temperature was consistent with water desorption temperature, because HCl was possibly adsorbed on water or interacted with water molecules via hydrogen bonds. Besides, the desorption temperatures of VC on Ru/TiO_2 were 220, 307, and 673 °C after water vapor introduction, which was mainly related to the advance of the oxygen species, and the desorption temperatures of Cl_2 and HCl were also lower. What was distinctly different from Ru/WO_3 was that only a small amount of CH_3COOH and CO_2 and a large amount of CO were generated, mainly due to the fact that there may be no enough adsorbed oxygen to supply the consumed lattice oxygen. The Ru/WO_3 sample possessed a large amount of lattice oxygen and could still produce a large amount of CO_2 in the absence of the complementary adsorbed oxygen, despite of the inevitable generation of CO.

In summary, the serious competitive adsorption between water and oxygen or 1,2-DCE at the oxygen vacancies was an important reason for the inhibition of activity, a result due to the hydrophilicity of Ru/TiO_2. The lattice oxygen activity of Ru/TiO_2 was high, and needed the adsorbed oxygen to supplement the oxygen vacancies in a timely manner once the reaction consumed the lattice oxygen. However, although the OOH species could be generated at the oxygen vacancies after the introduction of water vapor, the competitive adsorption of water led to the insufficient oxygen supplementation. In this conclusion, we eliminated the factor that the generated chlorine- and carbon-containing intermediate products were strongly adsorbed at the oxygen vacancies by recording the surface Cl 2p spectra of the Ru/TiO_2 sample after 10 h of reaction in the presence or absence of water vapor (Fig. S10). Ru/TiO_2, as an industrial catalyst for the Deacon process, shows good resistance to the chlorine species. There was no obvious accumulation of the chlorine species on the Ru/TiO_2 surface, as compared with that on the Ru/WO_3 surface. However, the cleaning effect of water on the sample surface was not observed in the XPS characterization. The O 1s, Ru 3d, W 4f, and Ti 2p XPS spectra of the fresh and used Ru/WO_3 and Ru/TiO_2 samples for 1,2-DCE or (1,2-DCE + H_2O) oxidation are shown in Fig. 10. The O_{ads}/O_{latt} molar ratio was estimated by quantitatively analyzing the XPS spectrum of each sample. The O_{ads}/O_{latt} molar ratio increased from 0.17 on the fresh Ru/WO_3 sample to 0.20 and 0.29 after 1,2-DCE and (1,2-DCE + H_2O) oxidation, respectively. The catalyst surface possessed a more amount of the adsorbed oxygen species, further indicating that the introduction of water to the reaction system could provide the active adsorbed oxygen species. For the Ru/TiO_2 samples, the O_{ads}/O_{latt} molar ratio was 0.16 in the presence of absence of water. Therefore, 1,2-DCE oxidation obeyed a MvK mechanism over the Ru/TiO_2 sample and a synergism of Langmuir−Hinshelwood (L−H) and MvK mechanisms over the Ru/WO_3 sample. The Ru in the fresh Ru/WO_3 catalyst mainly existed in the tetra- and hexavalent states. After 10 h of the high-temperature reaction, however, intensity of the Ru^0 species on the surface of Ru/WO_3 after (1,2-DCE + H_2O) oxidation increased, indicating that there was an electron transfer between Ru^0 and $Ru^{4+/6+}$. Over the Ru/TiO_2 catalyst, the Ru mainly existed in the form of Ru^0 as well as there was a small amount of Ru^{6+}, and almost no effect on the change in Ru valence state on the catalyst surface after 10 h of the on-stream reaction, but the changes of the Ti $2p_{3/2}$ and Ti $2p_{1/2}$ XPS spectra further indicate that the charge transfer might mainly occur at the Ti atom in Ru/TiO_2, while it took place at the metallic Ru^0 in Ru/WO_3 during the 1,2-DCE oxidation process. Ti^{3+} species existed in all of the Ru/TiO_2 samples, since the binding energy (458.2 eV) of Ti $2p_{3/2}$ was lower than that (459.2 eV) of the stoichiometric TiO_2 [47]. After the oxidation of 1,2-DCE, both W and Ti XPS signals on the surface of the catalyst were shifted to higher binding energy positions, which means that both W and Ti displayed higher oxidation states. As the support of the catalysts prepared in the present work, WO_3 has several advantages: (i) It possessed the ability to activate oxygen species [48,49] since WO_3 showed desorption of lattice oxygen and good surface oxygen species adsorption capacity at low temperatures; (ii) it contained the active hydroxyl groups [50], and the hydroxyl groups could provide adsorption and reaction sites for 1,2-DCE molecules; and (iii) it possessed abundant Brønsted acid sites. Ru mainly provided the Lewis acid site, while WO_3 mainly provided the Brønsted acid site that could influence the adsorption of CVOCs. The Brønsted acid sites of the sample were related to desorption of the chlorine species and tended to produce HCl, but a large amount of Cl_2 was still produced over Ru/WO_3, although Ru/WO_3 possessed the relatively stronger Brønsted acid sites than Ru/TiO_2 (Fig. S11). The similar phenomenon means that the Deacon reaction was dominant on the support with a

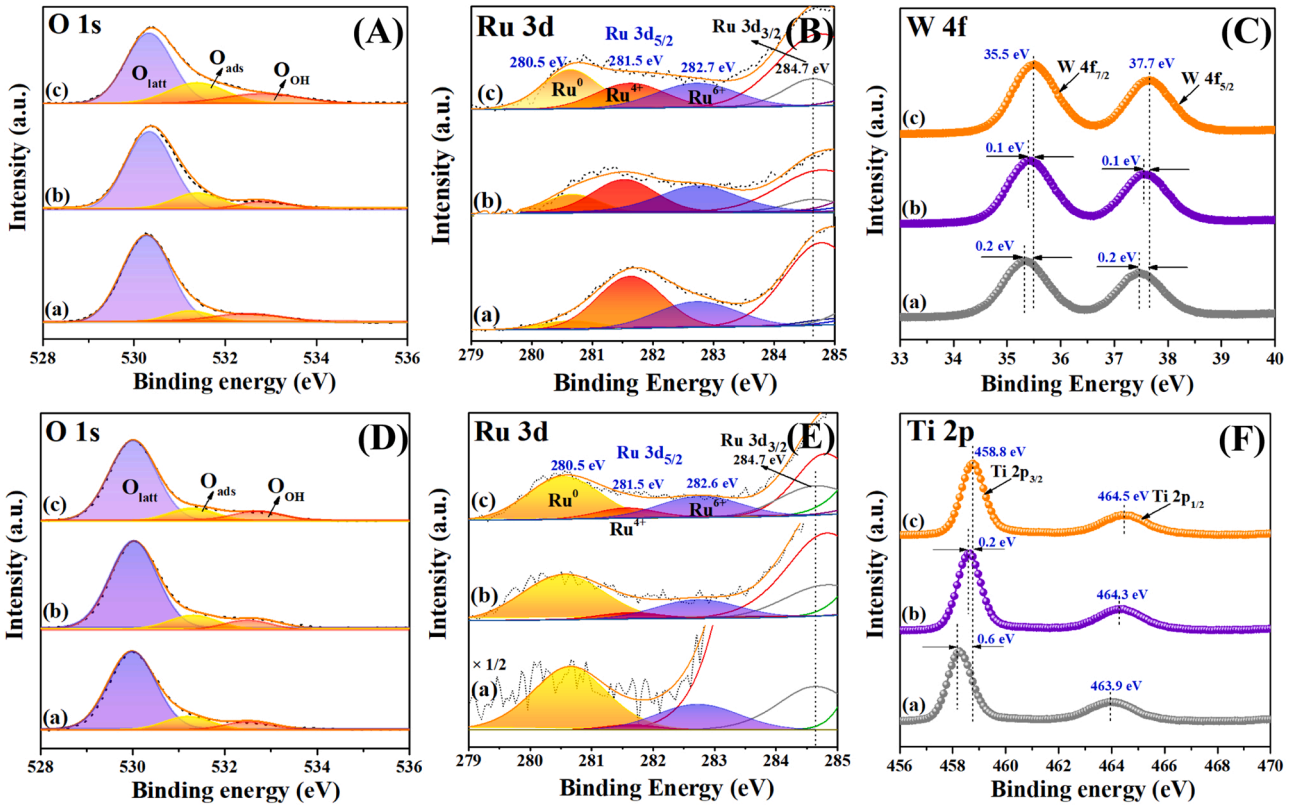

Fig. 10. O 1s, Ru 3d, W 4f, and Ti 2p XPS spectra of the (a) fresh and used (A–C) Ru/WO_3 and (D–F) Ru/TiO_2 samples after 10 h of (b) 1,2-DCE or (c) (1,2-DCE + H_2O) oxidation at 360 °C.

strong acidity [20]. Hence, adding appropriate water vapor to the reaction system could improve HCl selectivity by producing a more amount of the active oxygen species on Ru/TiO_2 or Ru/WO_3. However, the decline in 1,2-DCE oxidation activity was inevitable on Ru/TiO_2.

4. Conclusions

In this work, effects of water vapor on oxygen species, reaction pathways, and by-products distributions as well as accumulation of the chlorine species and carbon species on the Ru/WO_3 or Ru/TiO_2 surface for the oxidation of 1,2-DCE were deeply investigated using the isotopic strategy. After introducing water vapor, there were more amounts of the O_2^- and O^- species on the Ru/WO_3 surface, and isotope experiment results reveal the formation of $^{16}O^{18}O$ by the exchange of the oxygen species between water and catalyst. The presence of $C^{18}O$ at 287 °C directly confirms that the oxygen in water promoted the transformation of VC to CH_3COOH by tracing the reaction intermediate on Ru/WO_3, followed by the gradual consumption of hydroxyl groups and water adsorbed on it. The calculated Mulliken atomic charges reveal the mechanism of water attacking the VC, indicating that C1 and C2 are bonded with H and nucleophilic oxygen of −OH in sequence. Thus, the C═C bond in VC is broken and forms an unstable carbocation with a vacant orbital, followed by formation of the CH_3-CHCl-O− species that are readily oxidized to acetaldehyde and acetic acid. There was no doubt that water provided the active species and promoted the conversion of 1,2-DCE, and the in situ DRIFTS studies also indicate that water only tended to produce the relatively few chlorine-containing by-products and did not change the reaction pathways. The synergistic L−H and MvK mechanisms existed in the oxidation of 1,2-DCE in the presence of water vapor, most of the water was adsorbed at the hydroxyl groups on the sample surface, and the competitive adsorption at the active sites was weak on the Ru/WO_3 sample. However, the serious competitive adsorption between water and oxygen or 1,2-DCE at the oxygen vacancies was an important reason for the inhibition of activity due to the hydrophilicity of Ru/TiO_2, there was no enough adsorbed oxygen to supplement the oxygen vacancies in a timely manner and impeded the activation of oxygen molecules, although the OOH species could be generated in the oxygen vacancies, so the negative effect of the competitive adsorption was greater than the positive effect of the OOH species providing the reactive oxygen on the Ru/TiO_2 sample. Hence, water could participate in the reaction in the form of the active species, rather than a simple cleaning function, and the competitive adsorption of water and oxygen species was also a factor that is considered under practical industrial hydrophilic conditions.

CRediT authorship contribution statement

Xiaohui Yu: Investigation, Writing – review & editing. **Lingyun Dai:** Writing – review & editing, Methodology. **Jiguang Deng:** Writing – review & editing, Supervision, Project administration. **Yuxi Liu:** Investigation. **Lin Jing:** Investigation. **Xing Zhang:** Investigation, Data curation. **Ruyi Gao:** Investigation, Data curation. **Zhiquan Hou:** Investigation, Data curation. **Hongxing Dai:** Writing – review & editing, Supervision, Project administration.

Declaration of Competing Interest

The authors declare that they have no known competing financial interests or personal relationships that could have appeared to influence the work reported in this paper.

Acknowledgements

This work was supported by the National Natural Science Foundation Committee of China–Liaoning Provincial People's Government Joint Fund (U1908204), National Natural Science Foundation of China

(21876006, 21976009, and 21961160743), Foundation on the Creative Research Team Construction Promotion Project of Beijing Municipal Institutions (IDHT20190503), Natural Science Foundation of Beijing Municipal Commission of Education (KM201710005004), and Development Program for the Youth Outstanding–Notch Talent of Beijing Municipal Commission of Education (CIT&TCD201904019).

Appendix A. Supporting information

Supplementary data associated with this article can be found in the online version at doi:10.1016/j.apcatb.2021.121037.

References

[1] P. Yang, S.K. Fan, Z.Y. Chen, G.F. Bao, S.F. Zuo, C.Z. Qi, Synthesis of Nb2O5 based solid superacid materials for catalytic combustion of chlorinated VOCs, Appl. Catal. B 239 (2018) 114–124.
[2] Y. Yang, H. Li, H. Zhao, R.Y. Qu, S. Zhang, W.S. Hu, X.N. Yu, X.B. Zhu, S.J. Liu, C. H. Zheng, X. Gao, Structure and crystal phase transition effect of Sn doping on anatase TiO2 for dichloromethane decomposition, J. Hazard. Mater. 371 (2019) 156–164.
[3] L. Xu, E.E. Stangland, M. Mavrikakis, A. DFT, study of chlorine coverage over late transition metals and its implication on 1,2-dichloroethane hydrodechlorination, Catal. Sci. Technol. 8 (2018) 1555–1563.
[4] C. He, J. Cheng, X. Zhang, M. Douthwaite, S. Pattisson, Z.P. Hao, Recent advances in the catalytic oxidation of volatile organic compounds: a review based on pollutant sorts and sources, Chem. Rev. 119 (2019) 4471–4568.
[5] M.J. Tian, C. He, Y.K. Yu, H. Pan, L. Smith, Z.Y. Jiang, N.B. Gao, Y.F. Jian, Z. P. Hao, Q. Zhu, Catalytic oxidation of 1,2-dichloroethane over three-dimensional ordered meso/macroporous Co3O4/La0.7Sr0.3Fe0.5Co0.5O3: destruction route and mechanism, Appl. Catal. A 553 (2018) 1–14.
[6] C.T. Yang, G. Miao, Y.H. Pi, Q.B. Xia, J.L. Wu, Z. Li, J. Xiao, Abatement of various types of VOCs by adsorption/catalytic oxidation: a review, Chem. Eng. J. 370 (2019) 1128–1153.
[7] W. Zou, B. Gao, Y.S. Ok, L. Dong, Integrated adsorption and photocatalytic degradation of volatile organic compounds (VOCs) using carbon-based nanocomposites: a critical review, Chemosphere 218 (2019) 845–859.
[8] X.Y. Wang, Q. Kang, D. Li, Catalytic combustion of chlorobenzene over MnOx–CeO2 mixed oxide catalysts, Appl. Catal. B 86 (2009) 166–175.
[9] X. Zhang, Y.X. Liu, J.G. Deng, X.H. Yu, Z. Han, K.F. Zhang, H.X. Dai, Alloying of gold with palladium: an effective strategy to improve catalytic stability and chlorine-tolerance of the 3DOM CeO2-supported catalysts in trichloroethylene combustion, Appl. Catal. B 257 (2019), 117879.
[10] J. Su, W.Y. Yao, Y. Liu, Z.B. Wu, The impact of CrOx loading on reaction behaviors of dichloromethane (DCM) catalytic combustion over Cr-O/HZSM-5 catalysts, Appl. Surf. Sci. 396 (2017) 1026–1033.
[11] S. Albonetti, J.E. Mengou, F. Trifirò, Polyfunctionality of DeNOx catalysts in other pollutant abatement, Catal. Today 119 (2007) 295–300.
[12] Y.F. Gu, T. Cai, X.H. Gao, H.Q. Xia, W. Sun, J. Zhao, Q.G. Dai, X.Y. Wang, Catalytic combustion of chlorinated aromatics over WOx/CeO2 catalysts at low temperature, Appl. Catal. B 248 (2019) 264–276.
[13] X.H. Yu, L.Y. Dai, J.G. Deng, Y.X. Liu, L. Jing, X. Zhang, X.Y. Jiang, Z.Q. Hou, J. Wang, H.X. Dai, Catalytic performance and intermediates identification of trichloroethylene deep oxidation over Ru/3DOM SnO2 catalysts, J. Catal. 400 (2021) 310–324.
[14] Y.J. Lao, N.X. Zhu, X.X. Jiang, J. Zhao, Q.G. Dai, X.Y. Wang, Effect of Ru on the activity of Co3O4 catalysts for chlorinated aromatics oxidation, Catal. Sci. Technol. 8 (2018) 4797–4811.
[15] X.L. Weng, Y.H. Xue, J.K. Chen, Q.J. Meng, Z.B. Wu, Elimination of chloroaromatic congeners on a commercial V2O5–WO3/TiO2 catalyst: the effect of heavy metal Pb, J. Hazard. Mater. 387 (2020), 121705.
[16] F. Bertinchamps, C. Grégoire, E.M. Gaigneaux, Systematic investigation of supported transition metal oxide based formulations for the catalytic oxidative elimination of (chloro)-aromatics: Part II: influence of the nature and addition protocol of secondary phases to VOx/TiO2, Appl. Catal. B 66 (2006) 10–22.
[17] Q.G. Dai, J.Y. Wang, W. Deng, J.S. Hu, Q.Q. Wu, L.M. Guo, W. Sun, W.C. Zhan, X. Y. Wang, Comparative studies of P/CeO2 and Ru/CeO2 catalysts for catalytic combustion of dichloromethane: from effects of H2O to distribution of chlorinated by-products, Appl. Catal. B 111–112 (2012) 141–149.
[18] X. Zhang, L.Y. Dai, Y.X. Liu, J.G. Deng, L. Jing, Z.W. Wang, W.B. Pei, X.H. Yu, J. Wang, H.X. Dai, Effect of support nature on catalytic activity of the bimetallic RuCo nanoparticles for the oxidative removal of 1,2-dichloroethane, Appl. Catal. B 285 (2021), 119804.
[19] J. Zhao, W.J. Xi, C.S. Tu, Q.G. Dai, X.Y. Wang, Catalytic oxidation of chlorinated VOCs over Ru/TixSn1–x catalysts, Appl. Catal. B 263 (2020), 118237.
[20] J. Zhao, C.S. Tu, W. Sun, H.Q. Xia, H. Zhang, Q.G. Dai, X.Y. Wang, Catalytic combustion of CH2Cl2 over SO42−/TiSn1–x modified with Ru, Catal. Sci. Technol. 10 (2019) 742–756.
[21] Q.G. Dai, K. Shen, W. Deng, Y.P. Cai, J.R. Yan, J.Y. Wu, L.M. Guo, R. Liu, X. Y. Wang, W.C. Zhan, HCl-tolerant HxPO4/RuOx−CeO2 catalysts for extremely efficient catalytic elimination of chlorinated VOCs, Environ. Sci. Technol. 55 (2021) 4007–4016.
[22] H. Liu, J. Yang, Y.Y. Jia, Z.Q. Wang, M.X. Jiang, K. Shen, H.L. Zhao, Y.L. Guo, Y. Guo, L. Wang, S. Dai, W.C. Zhan, Significant improvement of catalytic performance for chlorinated volatile organic compound oxidation over RuOx supported on acid-etched Co3O4, Environ. Sci. Technol. 55 (2021) 10734–10743.
[23] Y.F. Gu, X.X. Jiang, W. Sun, S.X. Bai, Q.G. Dai, X.Y. Wang, 1,2-Dichloroethane deep oxidation over bifunctional Ru/CexAly catalysts, ACS Omega 3 (2018) 8460–8470.
[24] C.E. Hetrick, F. Patcas, M.D. Amiridis, Effect of water on the oxidation of dichlorobenzene over V2O5/TiO2 catalysts, Appl. Catal. B 101 (2011) 622–628.
[25] Y. Dai, X.Y. Wang, Q.G. Dai, D. Li, Effect of Ce and La on the structure and activity of MnOx catalyst in catalytic combustion of chlorobenzene, Appl. Catal. B 111–112 (2012) 141–149.
[26] T. Cai, H. Huang, W. Deng, Q.G. Dai, W. Liu, X.Y. Wang, Catalytic combustion of 1,2-dichlorobenzene at low temperature over Mn-modified Co3O4 catalysts, Appl. Catal. B 166–167 (2015) 393–405.
[27] Q.G. Dai, S.X. Bai, H. Li, W. Liu, X.Y. Wang, G.Z. Lu, Catalytic total oxidation of 1,2-dichloroethane over highly dispersed vanadia supported on CeO2 nanobelts, Appl. Catal. B 168–169 (2015) 141–155.
[28] Q.G. Dai, L.L. Yin, S.X. Bai, W. Wang, X.Y. Wang, X.Q. Gong, G.Z. Lu, Catalytic total oxidation of 1,2-dichloroethane over VOx/CeO2 catalysts: further insights via isotopic tracer techniques, Appl. Catal. B 182 (2016) 598–610.
[29] C. Ma, C.G. Yang, B. Wang, C. Chen, F.B. Wang, X.L. Yao, M.Y. Song, Effects of H2O on HCHO and CO oxidation at room-temperature catalyzed by MCo2O4 (M = Mn, Ce and Cu) materials, Appl. Catal. B 254 (2019) 76–85.
[30] Q.G. Dai, X.Y. Wang, G.Z. Lu, Low-temperature catalytic combustion of trichloroethylene over cerium oxide and catalyst deactivation, Appl. Catal. B 81 (2008) 192–202.
[31] F. Bertinchamps, A. Attianese, M.M. Mestdagh, E.M. Gaigneaux, Catalysts for chlorinated VOCs abatement: multiple effects of water on the activity of VOx based catalysts for the combustion of chlorobenzene, Catal. Today 112 (2006) 165–168.
[32] X.H. Yu, L.Y. Dai, Y. Peng, J.G. Deng, Y.X. Liu, L. Jing, X. Zhang, Z.Q. Hou, J. Wang, H.X. Dai, High selectivity to HCl for the catalytic removal of 1,2-dichloroethane over RuP/3DOM WOx: insights into the effects of P-doping and H2O introduction, Environ. Sci. Technol. 55 (2021) 14906–14916.
[33] M. Anpo, M. Che, B. Fubini, E. Garrone, E. Giamello, M.C. Paganini, Generation of superoxide ions at oxide surfaces, Top. Catal. 8 (1999) 189–198.
[34] R.F. Howe, Electron paramagnetic resonance studies of some supported organometallic catalysts, J. Chem. Soc., Faraday Trans. I 71 (1975) 1689.
[35] R. Prabhakaran, V. Krishnan, A. Geetha, H. Bertagnolli, K. Natarajan, Synthesis, EPR, electrochemistry and EXAFS studies of ruthenium (III) complexes with a symmetrical tetradentate N2O2 schiff base, Inorg. Chim. Acta 359 (2006) 1114–1120.
[36] K.L. Cao, H. Yang, S.X. Bai, Y. Xu, C.Y. Yang, Y. Wu, M. Xie, T. Cheng, Q. Shao, X. Q. Huang, Efficient direct H2O2 synthesis enabled by PdPb nanorings via inhibiting the O–O bond cleavage in O2 and H2O2, ACS Catal. 11 (2021) 1106–1118.
[37] M.M.R. Feijen-Jeurissen, J.J. Jorna, B.E. Nieuwenhuys, G. Sinquin, C. Petit, J. P. Hindermann, Mechanism of catalytic destruction of 1,2-dichloroethane and trichloroethylene over γ-Al2O3 and γ-Al2O3 supported chromium and palladium catalysts, Catal. Today 54 (1999) 65–79.
[38] X.L. Xu, L. Liu, Y.Y. Tong, X.Z. Fang, J.W. Xu, D. Jiang, X. Wang, Facile Cr3+-doping strategy dramatically promoting Ru/CeO2 for low-temperature CO_2 methanation: unraveling the roles of surface oxygen vacancies and hydroxyl groups, ACS Catal. 11 (2021) 5762–5775.
[39] Y. Guo, S. Mei, K. Yuan, D.J. Wang, H.C. Liu, C.H. Yan, Y.W. Zhang, Low-temperature CO_2 methanation over CeO2-Supported Ru single atoms, nanoclusters, and nanoparticles competitively tuned by strong metal–support interactions and H-spillover effect, ACS Catal. 8 (2018) 6203–6215.
[40] P. Panagiotopoulou, D.I. Kondarides, X.E. Verykios, Mechanistic study of the selective methanation of CO over Ru/TiO2 catalyst: identification of active surface species and reaction pathways, J. Phys. Chem. C 115 (2011) 1220–1230.
[41] J.C. Liu, Y. Tang, C.R. Chang, Y.G. Wang, J. Li, Mechanistic insights into propene epoxidation with O2–H2O mixture on Au7/α-Al2O3: a hydroproxyl pathway from ab initio molecular dynamics simulations, ACS Catal. 6 (2016) 2525–2535.
[42] D.G. Barton, S.G. Podkolzin, Kinetic study of a direct water synthesis over silica-supported gold nanoparticles, J. Phys. Chem. B 109 (2005) 2262–2274.
[43] C.R. Chang, X.F. Yang, B. Long, J. Li, A water-promoted mechanism of alcohol oxidation on a Au(111) surface: understanding the catalytic behavior of bulk gold, ACS Catal. 3 (2013) 1693–1699.
[44] C.R. Chang, Y.G. Wang, J. Li, Theoretical investigations of the catalytic role of water in propene epoxidation on gold nanoclusters: a hydroperoxyl-mediated pathway, Nano Res. 4 (2011) 131–142.
[45] D.M.P. Ferrandez, I.H. Fernandez, M.P.G. Teley, M.H.J.M. de Croon, J.C. Schouten, T.A. Nijhuis, Kinetic study of the selective oxidation of propene with O2 over Au–Ti catalysts in the presence of water, J. Catal. 330 (2015) 396–405.
[46] L.L. Yin, G.Z. Lu, X.Q. Gong, A. DFT, U study of the catalytic degradation of 1,2-dichloroethane over CeO2, Phys. Chem. Chem. Phys. 20 (2018) 5856–5864.
[47] A.M. Abdel-Mageed, K. Wiese, M. Parlinska-Wojtan, J. Rabeah, A. Brückner, R. J. Behm, Encapsulation of Ru nanoparticles: modifying the reactivity toward CO and CO_2 methanation on highly active Ru/TiO2 catalysts, Appl. Catal. B 270 (2020), 118846.

[48] D.L. Liu, C.H. Wang, Y.F. Yu, B.H. Zhao, W.C. Wang, Y.H. Du, B. Zhang, Understanding the nature of ammonia treatment to synthesize oxygen vacancy-enriched transition metal oxide, Chem 5 (2019) 376–389.
[49] X.D. Wu, L. Zhang, D. Weng, S. Liu, Z.C. Si, J. Fan, Total oxidation of propane on Pt/WOx/Al2O3 catalysts by formation of metastable Ptδ+ species interacted with WOx clusters, J. Hazard. Mater. 225–226 (2012) 146–154.
[50] W.M. Liao, X.X. Fang, B.H. Cen, J. Chen, Y.R. Liu, M.F. Luo, J.Q. Lu, Deep oxidation of propane over WO3-promoted Pt/BN catalysts: the critical role of Pt–WO3 interface, Appl. Catal. B 272 (2020), 118858.